

ORIGINAL ARTICLE

Open Access



# The Effect of Laser Ablation Pulse Width and Feed Speed on Necrosis and Surface Damage of Cortical Bone

Jose A. Robles-Linares<sup>†</sup>, Kieran Winter<sup>†</sup> and Zhirong Liao<sup>\*</sup>

## Abstract

Bone cutting is of importance in orthopaedic surgery but is also challenging due to its nature of brittleness—where severe mechanical and thermal damages can be introduced easily in conventional machining. Laser machining is a new technology that can allow for complex cut geometries whilst minimising surface defects i.e., smearing, which occur in mechanical methods. However, comparative studies on the influence of lasers with different pulse characteristics on necrotic damage and surface integrity have not been reported yet. This paper for the first time investigates the effects of laser type on the necrotic damage and surface integrity in fresh bovine cortical bone after ex-situ laser machining. Three lasers of different pulse widths, i.e., picosecond, nanosecond and continuous wave lasers have been investigated with different feed speeds tested to study the machining efficiency. The cutting temperature, and geometrical outputs have been measured to investigate the thermal influence on the cooling behaviour of the bone samples while high-speed imaging was used to compare the material removal mechanisms between a pulsed and continuous wave laser. Furthermore, an in-depth histological analysis of the subsurface has revealed that the nanosecond laser caused the largest necrotic depth, owing to the high pulse frequency limiting the dissipation of heat. It has also been observed that surface cracks positioned perpendicular to the trench direction were produced after machining by the picosecond laser, indicative of the photomechanical effect induced by plasma explosions. Therefore, the choice of laser type (i.e., in terms of its pulse width and frequency) needs to be critically considered for appropriate application during laser osteotomy with minimum damage and improved healing.

**Keywords:** Bone cutting, Necrosis, Surface damage, Laser machining, Histology

## 1 Introduction

Bone is an important tissue in the human body as it allows vital locomotive functions of humans to take place, such as providing stiffness, walking or jumping [1]. However, bones are also load-sensitive and semi-brittle [2, 3] and, therefore, prone to injuries. As a result, bone surgical interventions are a daily task in orthopaedics, neurosurgery, and dentistry. However, many of these involve

the mechanical material removal by principally cutting (i.e., milling, sawing, drilling) [4, 5] or abrading the tissue to perform the surgery (e.g., total knee arthroplasty, hole drilling, implant or screw insertion). Contrary to soft tissues which are largely elastic [5], bone is semi-brittle, implying that it can easily get damage induced to its subsurface [6] due to mechanical machining [7]; but bone also possess a unique self-healing capacity [8]. These two characteristics make bone an interesting and complex material from both an engineering and medical perspective, which makes tool design a difficult task [9, 10], but it can be better analysed by understanding its intricate hierarchical microstructure [11].

<sup>†</sup>Jose A. Robles-Linares and Kieran Winter contributed equally to this work and share first authorship

\*Correspondence: [zhirong.liao@nottingham.ac.uk](mailto:zhirong.liao@nottingham.ac.uk)

Faculty of Engineering, University of Nottingham, Nottingham NG7 2RD, UK

Bone can be broadly divided in two main types, which are the cortical tissue and the trabecular tissue, both of which are shown as a portion of a long bone structure shown in Figure 1. Out of these two, cortical bone is of vast interest since it possesses a superior mechanical strength and density over trabecular bone, thus it is of major relevance when it comes to machining. Cortical bone can be regarded as a natural biological composite material comprised of osteons (i.e., the equivalent to unidirectional fibres in conventional composites) immersed in the interstitial lamellae (i.e., the matrix in conventional composites), as shown in Figure 1. Additionally, the Volkmann's and Haversian canals, which carry the necessary nutrients for a proper bone function [12], provide a unique arrangement of a porosity system within the tissue. This is one of the reasons why scaffold and implant design is tailored or customised with a controlled porosity that resembles that of natural cortical bone [11], especially if employing additive manufacturing techniques for fabrication [13, 14].

As a biological tissue, bone possesses a cellular structure that maintains it in its living state with appropriate metabolism and remodelling (i.e., capacity to heal itself over time) functions. One of the cells involved in this process are osteocytes, which are trapped inside the bone in pits called lacunae (see Figure 1(b)) [15]. These cells,

among others, keep the bone in a healthy state and aid in the healing process after the tissue is exposed to damage (e.g., by machining-induced mechanical and/or thermal loads [7]).

The intricate microstructure in cortical bone results in a complex material from a machining perspective that makes bone a difficult material to cut, as it can behave both ductile or brittle, depending on the cutting parameters [2]. Thus, during conventional machining, the mechanical effect may induce sufficient strain that facilitates crack propagation from the cutting zone and into the material [16], or induce a brittle and weak layer in the machined subsurface at the micro-level [7]. Additionally, the cutting energy will also dissipate in the form of heat, and as a biological material, the cellular integrity of the tissue may be compromised if the temperature is high enough [17]. In general, if the tissue is exposed to a temperature of 47 or 50 °C during 60 or 30 seconds, respectively, necrosis (i.e., death of osteocytes) will occur, which implies that the healing, remodelling and metabolism functions will be hindered either temporarily or permanently [18]. Additionally, much less time is required for necrosis to occur if the temperatures are larger.

Since mechanical machining (e.g., milling, grinding, sawing) poses a great challenge in terms of machining-induced damage avoidance, non-conventional machining

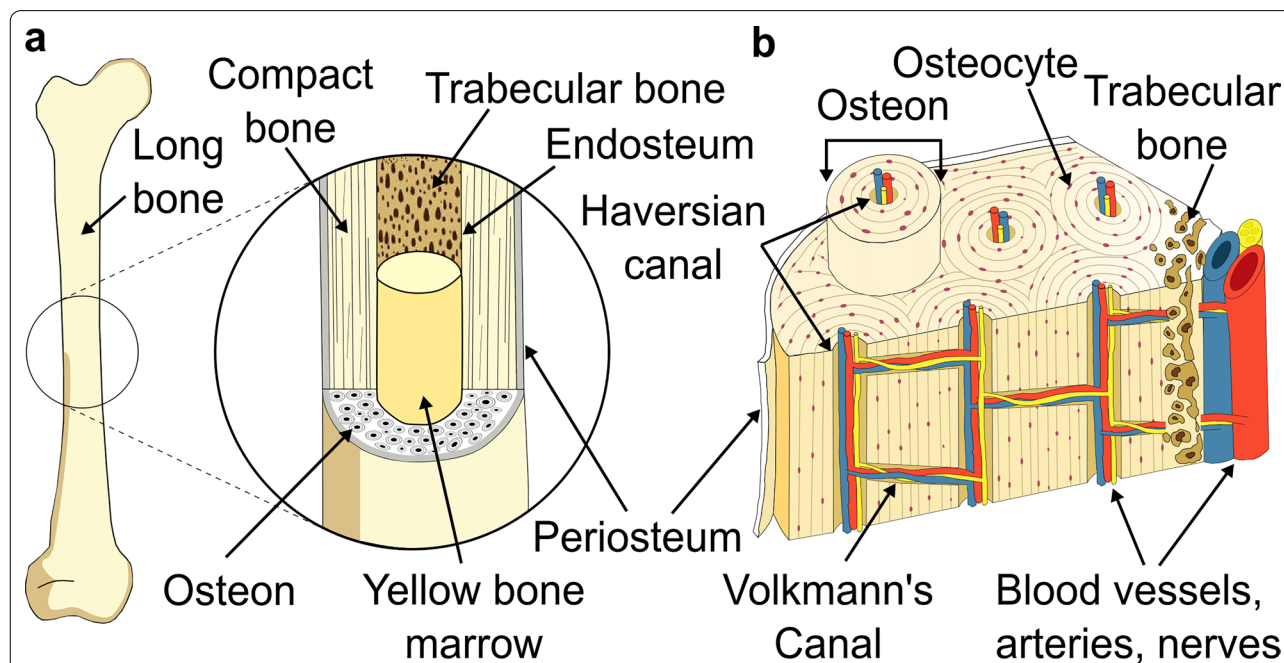


**Figure 1** Schematic overview of the bone structure: (a) a long bone possesses two main tissues, i.e., cortical bone in the outermost region and trabecular bone in the innermost region, which encloses the yellow bone marrow, (b) the cortical bone microstructure consists of osteons that run along the principal loading direction of the bone and are immersed in the interstitial lamellae. Inside the cortical tissue two main porosity systems (Haversian and Volkmann's) carry the necessary blood vessels and nerves for maintaining a healthy tissue. The osteocytes (shown as purple dots) are the cells that monitor the metabolism and remodelling process of the tissue. Schematic adapted from Ref. [11]

techniques could represent a promising approach towards improving the material response during machining. Laser (e.g., pulsed or continuous lasers) machining can remove material through a range of mechanisms. Pulsed laser ablation is a technique that removes material through the use of a high intensity, focused laser beam, with a short pulse width [19] which leads to energy absorption by the material, subsequently vaporising/ionising it. On the other hand, lasers with longer or continuous pulses may have fluencies below the ablation threshold—leading to a more thermally based material removal mechanism such as melting [20].

Additionally, laser machining provides an improved cutting geometry and precision over conventional tools due to reduced/no mechanical loads [21]. Therefore, laser ablation represents a non-conventional machining approach that could improve the bone cutting process by eliminating the mechanical effect. However, the thermal and shock waves from the laser beam can propagate deep into the bone, thus resulting in possible damage even in regions far from the machined or ablated zone [22]. Due to the fully thermal phenomenon and considering the low thermal conductivity of bone [23], necrosis becomes more relevant.

The three most common lasers used in hard tissues, like cortical bone, are CO<sub>2</sub>, Er:YAG and Nd:YAG types. The reason for these relies on the optical absorption properties of the tissue, and more specifically, on the ones from its individual constituents (e.g., water, collagen) [24]. For instance, the CO<sub>2</sub> laser wavelength (i.e., 10.6 μm) is within the optical absorption spectrum of hydroxyapatite (i.e., 9–11 μm) [25], one of the most important constituents from the bone's mineral, being the mineral phase the main constituent of bone [26]. The wavelength of Er:YAG lasers (i.e., 2.94 μm) is similar to one of the largest absorption peaks of water (ca. 3 μm), the third main constituent of bone [26]. The wavelength from Nd:YAG lasers is 1.094 μm, but this value can be shortened by frequency doubling, meaning that it can be tailored to minimise water absorption [27], thus maximising the laser penetration depth into the tissue in water-rich (e.g., with coolant) environments.

Rayan et al. [28] did *in vivo* CO<sub>2</sub> laser cutting without coolants in cortical bone and reported that tissue carbonisation is easily induced along with necrosis; however, the laser pulse width was kept constant at 0.1 ms along with a frequency of 2 kHz. Krause et al. [25], also using a CO<sub>2</sub> laser without coolants, reported a necrotic depth ranging from 30 to 200 μm when the laser energy density is within 160–2062 J/cm<sup>2</sup>; however, a comprehensive assessment is hindered since the pulse width (5 ms, 10 ms and continuous) and frequency (10 Hz, 20 Hz, continuous) varied for each energy density condition. Frentzen et al. [29] also

employed a CO<sub>2</sub> laser (80 μs pulse width) in *ex-vivo* bone cutting, but due to the usage of external coolant (fine air-water spray), both necrosis and tissue carbonisation were totally avoided.

Since laser machining implies a lower material removal rate as opposed to conventional machining, studies on improving the cutting efficiency in cortical bone have also been explored. For instance, a research using an Er:YAG laser (300 μs pulse width and 20 Hz frequency) [30] proposed a set of laser processing parameters that could result in lower cutting time, when compared to conventional drilling, even producing less heat. However, the laser was coupled with a water spray cooling system and the conventional drilling parameters were intentionally produced with a low speed, thereby hindering the understanding of the real material response both in terms of necrosis and cutting efficiency. Baek et al. [31] showed that mechanical machining, often resulting in a smear layer in the cut surface, blocks the bleeding of the bone, whereas laser machining eases the bleeding by leaving an open wound without smearing on top; this is the reason why laser machining could result in an improved healing time. It is known that an increased pulse laser energy will inherently result in a larger ablation volume, but regarding the effect of pulse width, Beltran et al. [32] showed, in a limited width range (i.e., microsecond range, 244–388 μs) that there was no direct relation and instead proposed that the driving factor in the ablation efficiency is only the pulse energy. Additionally, Beltran et al. [33] explained how the ablation rate (i.e., ablated bone in depth per unit time) depends on both the feed speed and the number of passes of the laser beam, generally showing that for a single laser pass, the ablation rate increases while lowering the feed. However, they also suggested that a single pass results in a more uneven trench (i.e., with ripples), thereby showing that there is a non-trivial relationship between feed speed, cutting efficiency and surface quality.

Bone machining via non-conventional methods is under current investigations towards making the process a more reliable one in surgical environments. However, there is still lack of understanding on the relation between laser type (in terms of laser pulse width) and induced necrosis, as most of the aforementioned studies always employ cooling methods to the laser machining process. Additionally, most studies aiming on improving the cutting efficiency (i.e., maximising material removal rate per unit time) have been limited to a fixed pulsed width laser, thus making the processing recommendations pulse-width dependent. To bring more light into these aspects, here, the effect of pulse width of the laser beam on damage cortical bone both in terms of its surface characteristics (e.g., cracks, roughness) and necrosis

is investigated. This was done for an Nd-YAG laser with pulse widths in the nanosecond, picosecond, and continuous ranges. Additionally, various feed speeds (i.e., 0.25–45 mm/s) were employed to understand the machining efficiency of each case. Histological analysis was used as a gold standard technique for assessment of the necrotic depth after machining, while metrology equipment was used for evaluation of the machined trench profiles post-machining. In this paper, the relation of laser pulse width with necrosis inducement is shown to be non-trivial, highlighting that variations of pulse width can produce both carbonisation and necrotic damage, as well as mild machining with minimum damage. It is also shown that the use of pulse widths in the picosecond range can shift the material removal mechanism from thermal to opto-mechanical, thereby reducing the inducement of thermal damage.

## 2 Methods

### 2.1 Samples Acquisition and Preparation

A single mid-diaphysis from a bovine femur was used in this research due to its similarities with human bone in terms of its composition [34], its mechanical response to machining and the fact that it provides allowance of histological analysis for machining-induced necrosis [7]. The bone was acquired from a local butcher and was immediately cut to obtain prism shapes of  $15 \times 15 \times 15 \text{ mm}^3$  by under vast amounts of saline solution to preserve the tissue and its cells, as well as its mechanical integrity [35].

To obtain a flat surface suitable for the laser machining processes, all the samples were manually ground (Tegrapol-21, Struers) with a 1200 SiC grit to achieve a

final shape of  $5 \times 5 \times 5 \text{ mm}^3$ , again, while using abundant saline solution during the process. The samples were rinsed with fresh saline solution in an ultrasonic bath to remove any surface debris. Surface polishing was not performed to avoid any contamination that could compromise the cellular integrity of the tissue. When not in use, the samples were kept at  $-20 \text{ }^\circ\text{C}$  in a saline soaked gauze [36]. A total of 5 samples, including a control sample, were used for histological analysis, while a total of 27 samples were used for trench profile analysis.

### 2.2 Laser Ablation Tests

To machine the trenches, three laser types were used with varying pulse widths (Figure 2), i.e., picosecond pulsed, nanosecond pulsed, and continuous wave. The picosecond laser used was an Nd:YAG laser with an ultra-short pulse width of 60 ps with the pulse energy of 0.88 mJ and average power output at 3.5 W. For the histological evaluation, two feed speeds were selected [*Pico-Fast* (PF) = 5 mm/s, and *Pico-Slow* (PS) = 1 mm/s]. The continuous wave laser (i.e., non-pulsed) used was an Nd:YAG laser operating at 20% (19.5 W) of the maximum output power (measured at 97.5 W) and a feed speed of 20 mm/s (CW) was used to limit the total energy supplied to the sample. The nanosecond laser used was an Nd:YAG laser with the pulse energy of 0.52 mJ, average power output at 18.3 W, and a pulse width of 200 ns. A feed speed of 5 mm/s was used in the histological evaluation of the nanosecond laser sample (Nano) to provide comparison with both: (1) the total energy transferred to the sample in PS; and (2) the average output power in CW. The complete laser parameters can be found in Table 1. As a rule of thumb,

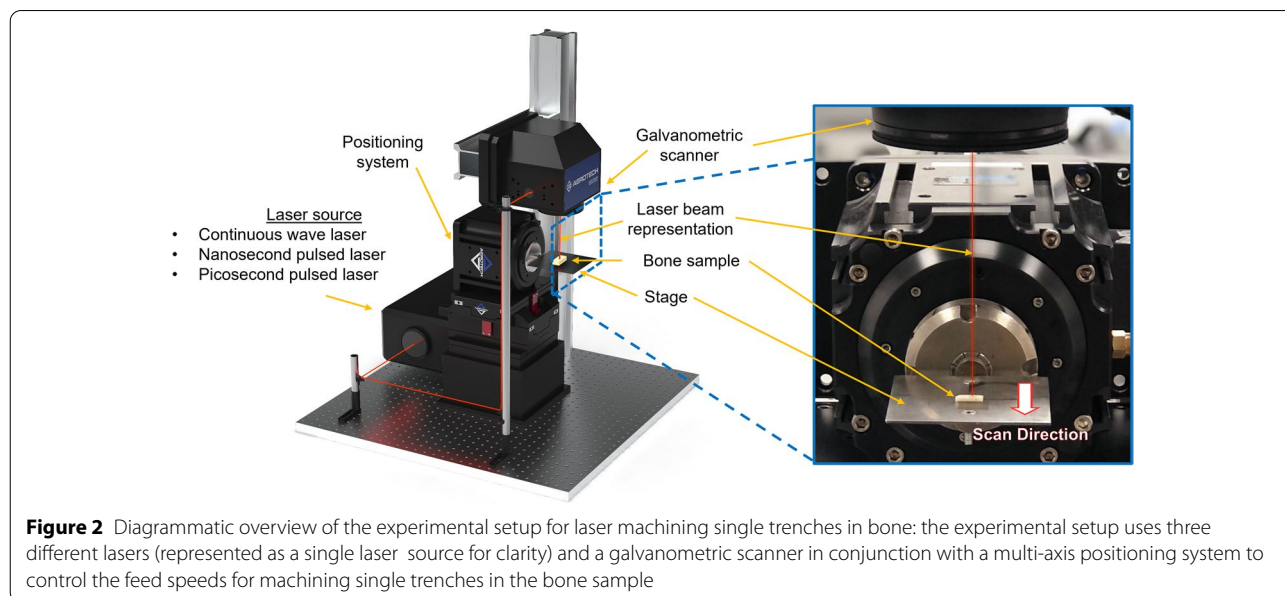


**Figure 2** Diagrammatic overview of the experimental setup for laser machining single trenches in bone: the experimental setup uses three different lasers (represented as a single laser source for clarity) and a galvanometric scanner in conjunction with a multi-axis positioning system to control the feed speeds for machining single trenches in the bone sample

**Table 1** Laser machining parameters for necrosis inspection

	PF	PS	CW	Nano
Laser type	Picosecond (fast feed)	Picosecond (slow feed)	Continuous Wave	Nanosecond
Wavelength (nm)	1064	1064	1090	1062
Pulse width (ps)	60	60	N/A	$2 \times 10^5$
Repetition rate (kHz)	4	4	N/A	35
Average output power (W)	3.5	3.5	19.5	18.3
Peak pulse power (kW)	$14.6 \times 10^3$	$14.6 \times 10^3$	N/A	2.6
Spot size ( $\mu\text{m}$ )	40.0	40.0	30.0	51.5
Pulse energy (mJ)	0.88	0.88	N/A	0.52
Feed (mm/s)	5	1	20	5
Trench length (mm)	3.5	3.5	3.5	3.5
Total pulses along trench length	2800	14000	N/A	24500
Total interaction time (s)	$1.68 \times 10^{-7}$	$8.40 \times 10^{-7}$	0.175	$4.90 \times 10^{-3}$
Total energy (J)	2.45	12.25	3.41	12.81

the laser processing parameters were determined by two primary factors: (1) avoidance of visible charring of the bone at low feed speeds; and (2) acceptable material removal efficiency at high feed speeds. The laser machining was completed without cooling/irrigation of the bone samples, they were conducted in a fresh state to understand the material behaviour and response to machining by different laser types as opposed to broadening the scope to become an exercise in process optimisation.

Temperature measurements were completed using the same laser parameters as the necrosis investigation (Table 1). The temperature was measured by infrared (IR) thermography using an FLIR A655SC Long Wavelength IR camera with a  $2.9 \times$  magnification lens attached and data was recorded at 50 Hz. To accurately record the temperature with the IR camera, the emissivity of the material must be known. Prior studies [37] have measured the emissivity of fresh bovine bone to be  $0.96 \pm 0.1$  at a temperature of 40 °C using the same FLIR A655SC camera, therefore, an emissivity of 0.95 for all experiments was employed. The camera is calibrated for three temperature profiles ( $-40$  °C to 150 °C (Figure 3(a)), 100 °C to 650 °C (Figure 3(b)), and 300 °C to 2000 °C (Figure 3(c))), as the temperature that the bone is elevated to during laser machining did not always remain in one of these profiles, the recording was repeated three times to obtain a dataset in each of the temperature profiles for each sample. This method facilitated the accurate temperature recording ( $\pm 2\%$  accuracy) at both: (1) the lower ( $\sim 50$  °C) region for investigating the spatial dissipation of heat, and (2) the higher ( $>1000$  °C) region for measuring the maximum instantaneous temperature. The data was processed using the ResearchIR Max software by FLIR where spatial measurements of the temperature relative to the radial distance from beam centre were measured

as well as the maximum temperature across a radial profile relative to time (Figure 3).

In order to understand the mechanisms of material removal taking place during the different laser processes, high-speed imaging using an IDT Y4 camera was completed for stationary drilling with the continuous wave and nanosecond-pulsed lasers.

### 2.3 Surface Inspection

To further evaluate the effects of the total interaction time between the laser and bone sample on the surface morphology after machining by each of the three laser types, single trenches were machined across a range of feed speeds,  $F$ , (mm/s) (Table 2). As the samples for this stage were prepared prior to the completion of the histological analysis, the upper ( $F_{\text{max}}$ ) and lower ( $F_{\text{min}}$ ) bounds were chosen based on the level of carbonisation observed visually by optical microscopy after iterative pre-experimental trials. More specifically, the  $F_{\text{min}}$  bounds were selected due to an elevated level of bone carbonisation whereas the  $F_{\text{max}}$  bounds typically had minimal discolouration. The  $F$  steps were subsequently calculated to ensure that a linear  $F$  range was evaluated over nine trenches for each of the three laser types. All the operating parameters not dependent on  $F$  for each of the lasers were kept identical to those used for the necrosis inspection (i.e., wavelength, pulse width, repetition rate, average power output, spot size, pulse energy).

Following the laser machining of the samples, 3D inspection of the trenches was completed using the Bruker Alicona InfiniteFocus G4. This was achieved by non-contact probing by focus variation which allowed for measurements of the trench depth and the surface morphology around the cut surface. The data was processed using the MountainsMap 7 Premium software

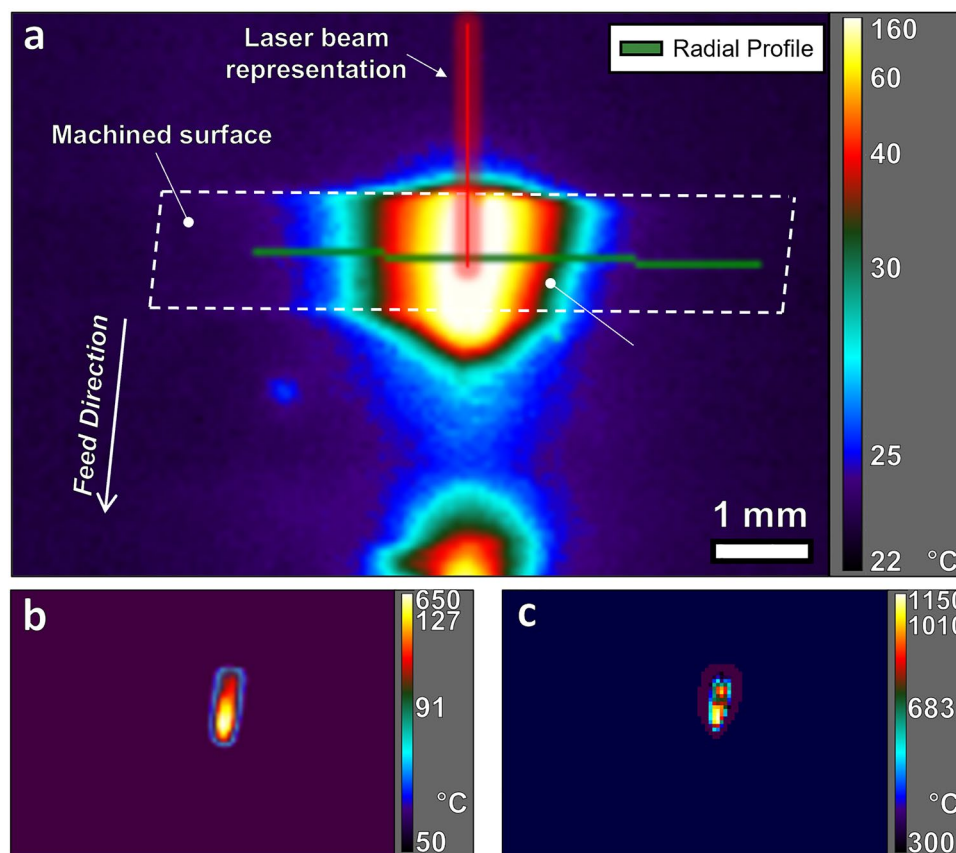


**Figure 3** Schematic overview of thermal imaging methodology: the schematic depicts the experimental methods used to investigate the thermal properties in the surface of the bone sample during laser machining. The radial profile is used for both the spatial and temporal plots. It should be noted that the colour bar is non-linear and uses plateau equalisation to improve the contrast for the entire scene. As there is not one camera calibration profile to cover the complete temperature range, three recordings were used: (a) low-range, (b) mid-range, (c) high range

**Table 2** Laser machining feed speeds for surface morphology inspection

Parameter	Picosecond	Nanosecond	Continuous wave
$F_{min}$ (mm/s)	0.25	2.50	5.00
$F_{max}$ (mm/s)	6.25	6.50	45.00
Step (mm/s)	0.75	0.50	5.00
Machined feature	Single trench	Single trench	Single trench

from Digital Surf. The scans were first levelled in the vertical direction based on the mean surface height of the unaffected areas surrounding the trench to obtain an accurate reference plane to measure the trench depth from. A series of cross-sectional profiles of the trench were taken to calculate the mean depth across the profile, these were subsequently plotted and centred on the maximum trench depth. The maximum trench depths for the range of feed speeds (Table 2) were also

studied to investigate the linearity of the trench depth relative to feed speed.

### 2.4 Histological Analysis

To make a necrosis assessment, histological analysis was performed on a set of 5 samples, including a control sample. The methodology for doing this has been documented in a previous work [7], but it mainly consists of a cellular fixation process using 10% neutral formalin, a 10-day decalcification process for softening the tissue, mounting all the samples in paraffin, sectioning the mounted samples with a microtome to obtain 7- $\mu$ m slices, an H&E staining process to allow improved morphological observation of the tissue and, finally, mounting the stained slices in a mixture of distyrene, plastic and xylene (i.e., DPX). This process yields microscopy slides with stained bone slices that are fit for analysis under light microscopy.

Image analysis and necrotic depth evaluation (i.e., measurement from the trench site to the disappared

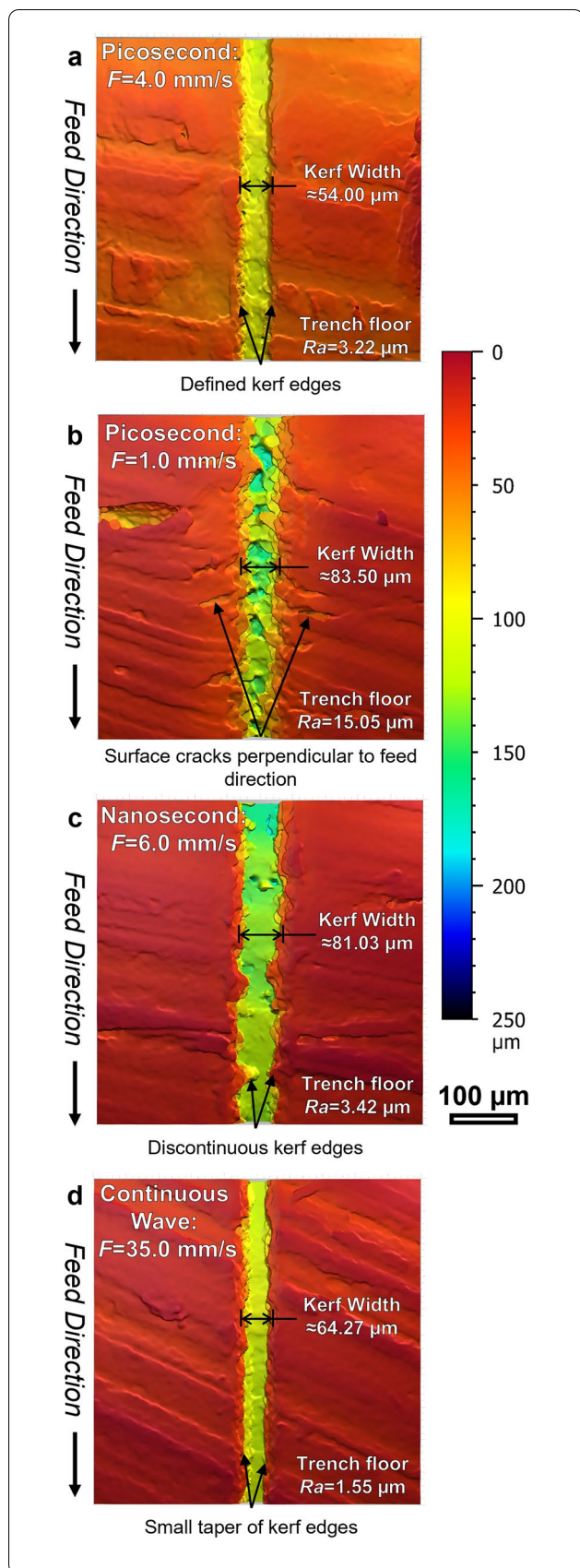


**Figure 4** Surface topography maps after laser machining: The surface topography maps observing a single trench machined by (a) the picosecond laser at a feed speed of 4.0 mm/s, (b) The picosecond laser at a feed speed of 1.0 mm/s where cracks that are propagating perpendicular to the feed direction from the kerf edges are visible, (c) The nanosecond laser at a feed speed of 6.0 mm/s, (d) The continuous wave laser at a speed of 35.0 mm/s

osteocytes extent) were made in Fiji (ImageJ). Additionally, a control sample (i.e., non-machined) was employed to confirm that the sample preparation process did not induce necrosis to the tissue. In total, 5–7 slices per sample were inspected.

### 3 Results

#### 3.1 Surface Quality Assessment

Surface integrity is an important aspect in conventional materials, such as metals [38], since the surface condition post-machining can alter the material behaviour in-service and possibly lead to early-stage failures if abusive cutting conditions occur [39]. In cortical bone this is also the case; thus, to understand the influence of laser type (in terms of pulse width) on the machining efficiency, a metrological assessment of the machined trench and bone surface was completed. Topological maps (see Figure 4) observing a plan view of the machined surface revealed the variation in single trench geometry for the laser types. Moreover, two feed speeds (1.0 mm/s and 4.0 mm/s) for samples machined by the picosecond laser to determine the extent to which feed speeds affect the single trench geometry and surface morphology for lasers in the same pulse width region.

It was found that the lowest kerf width (54  $\mu\text{m}$ ) was achieved by the picosecond laser at a feed speed of 4.0 mm/s (Figure 4(a)) which contrasted the slower picosecond laser ( $F = 1.0$  mm/s) (Figure 4(b)) that had a kerf width of (83.50  $\mu\text{m}$ )—a 55% increase. The kerf edges were also more defined in the faster picosecond laser than the slower, where the latter showed surface cracks propagating perpendicularly to the feed direction. The faster picosecond laser also produced a smoother trench floor ( $R_a = 3.22$   $\mu\text{m}$ ) than the slower ( $R_a = 15.05$   $\mu\text{m}$ ). This combination of well-defined kerf edges and a smoother trench floor in the faster picosecond sample suggests that for machining trenches with multiple passes, the decrease in single trench depth may be offset by optimised surface, i.e., the laser beam focus would be more controlled throughout multiple passes compared to a rougher surface where the undulations in surface height would not remain in optimal focus.

On the other hand, the kerf width of the trench machined by the nanosecond laser at a feed speed of 6.0 mm/s (Figure 4(c)) was measured at 81.03  $\mu\text{m}$ , which

was similar to that in the slower picosecond laser ( $F = 1.0$  mm/s), however the trench floor was similar in roughness ( $R_a = 3.42$   $\mu\text{m}$ ) to that of the faster picosecond laser ( $F = 4.0$  mm/s). Although the trench floor roughness in the sample machined by the continuous wave laser ( $F = 35.0$  mm/s) (Figure 4(d)) was the lowest measured ( $R_a = 1.55$   $\mu\text{m}$ ), there is a small kerf taper which widens the kerf width (64.27  $\mu\text{m}$ ) at the machined surface due to the convergence/divergence of the beam above and below the focal point.

If the machining efficiency was the only goal, then the key factors influencing the decision of laser type would be one which achieves a deep trench depth at a fast feed speed. From a clinical frame of reference however, this decision is more nuanced; requiring a higher weighting to be given to the later discussed necrotic damage (see Figure 9). To address the efficiency problem, the mean cross-sectional trench profiles were calculated (Figure 5) for the bone samples machined with identical parameters as those used in the histological assessment and curves plotting the mean trench depth over a range of feed speeds (Figure 6) were used to investigate the linearity of the relationship. The mean profile width of the nanosecond ( $F = 5$  mm/s) laser trench was the broadest due to the graduation of the kerf, whereas the continuous wave laser trench profile was the slenderest. It could be posited that a narrower kerf would be a beneficial characteristic of the laser in a clinical setting, allowing for precise cutting paths. This precision, however, would need to coincide with a high degree of predictability to be accurate. When the trench depth machined by the continuous wave laser is compared with feed speed (Figure 6), there is a low coefficient of determination between the variables ( $R^2 = 0.77$ ) compared to those machined by the picosecond laser and

nanosecond laser ( $R^2 = 0.90$  and  $R^2 = 0.93$  respectively). This leads to the implication that the reliability and stability of the laser source is an important factor to consider. For feed speeds  $> 3.5$  mm/s, the trenches machined by the nanosecond laser increase greatly in their depth, and the sharp decrease as feed speeds increase offer an exceptionally narrow window of operation for this laser despite the high fit. Conversely, over a similar range of feed speeds, the trench depths after machining by the picosecond laser occupied a far narrower span of depths whilst also maintaining a comparatively high fit.

To understand the causes non-linear relationship between trench depth and feed speed for the different laser types, an investigation into the thermal behaviour of the machined bone was completed (Figure 7). By plotting temperature across the radial profile taken at the time when the radius that was greater than  $50$   $^{\circ}\text{C}$  was at a maximum (Figure 7(a)), the thermal penetration depth can be considered. Comparing this spatial data with the temporal data (Figure 7(b)) measured across the same profile allows us to obtain a clearer understanding of the mechanisms which influence the machining efficiency and the level of necrosis. The distance where the temperature of the bone  $>50$   $^{\circ}\text{C}$  was the highest after machining by nanosecond laser (1550  $\mu\text{m}$ ) which is far greater than the samples cut by the other lasers. Despite the continuous wave laser increasing the surface temperature to  $1318$   $^{\circ}\text{C}$  compared to the nanosecond laser ( $830$   $^{\circ}\text{C}$ ), there is a far greater rate of cooling in the former. The distance that temperature was elevated  $>50$   $^{\circ}\text{C}$  after machining by the picosecond laser was substantially smaller for both tested feed speeds, which can be explained by the high rate of cooling observed in them after reaching their peak temperature. The low thermal penetration depth and high

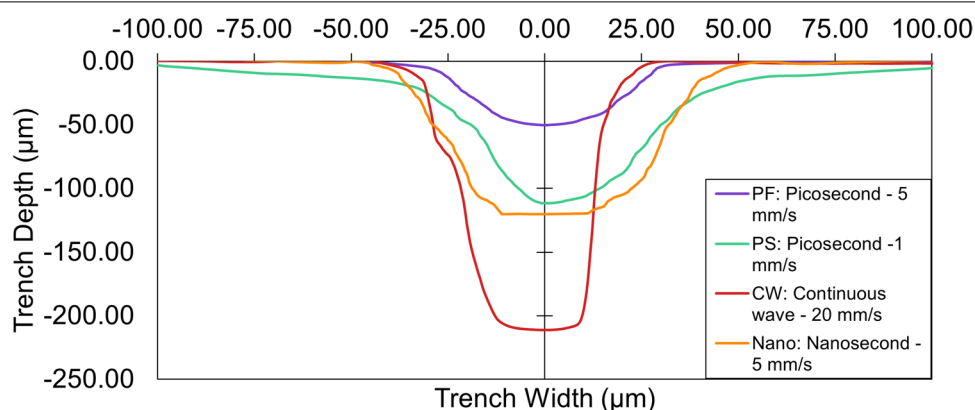


**Figure 5** Mean cross-sectional trench profile: the mean cross-sectional trench profiles were plotted for samples machined with identical process parameters as those used in the histological analysis

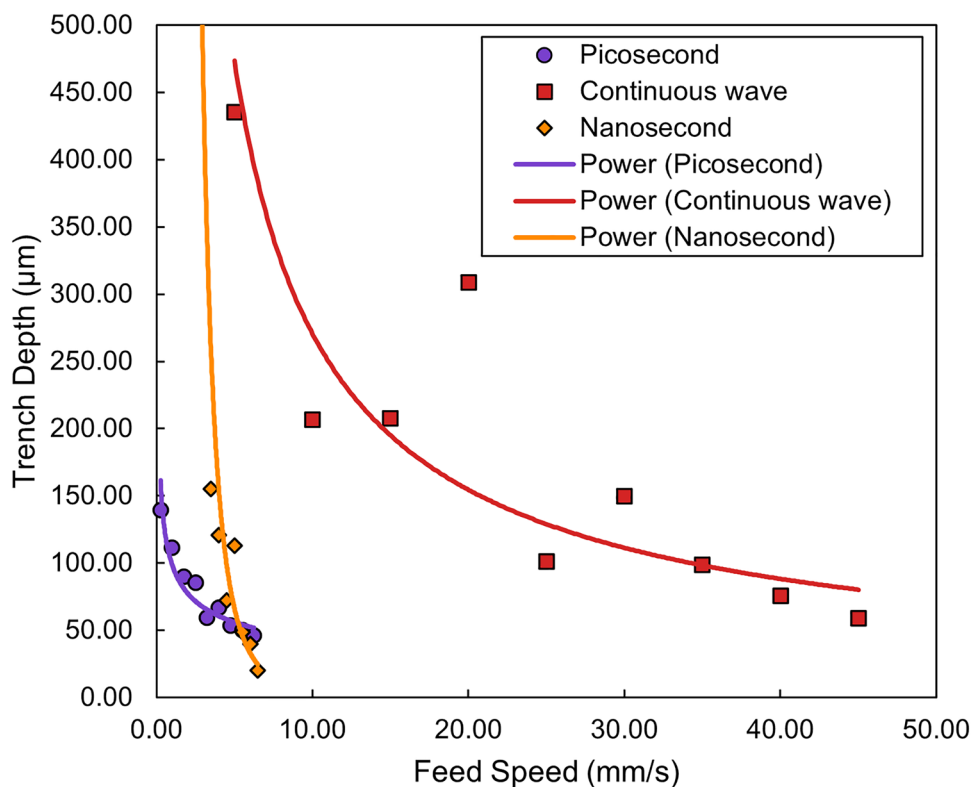


**Figure 6** Investigation into the effect of feed speed on the trench depth: the maximum trench depth taken from the mean cross-sectional profiles were plotted over a range of feed speeds to compare the efficiency and predictability of machining by the different laser types

cooling rate observed in the faster (5 mm/s) picosecond laser sample leads to the prediction of positive results in the later necrosis assessment.

Using high speed imaging whilst machining by the continuous wave laser and nanosecond pulsed laser, the difference in material removal mechanisms was observed (Figure 8). In the nanosecond pulsed laser (Figure 8(a)), the initiation of plasma generation (Figure 8(a)-(ii)) followed by the subsequent micro-explosions (Figure 8(a)-(iii)) caused pressure waves to propagate through the surface (Figure 8(a)-(iv)). These explosions cause the expansion of the plasma plume leading to the ejection of vapourised and melted material from the surface. On the other hand, machining with the continuous wave laser (Figure 8(b)) was not explosive, rather, the material removal was almost entirely a thermal mechanism. Some ionisation of the surface material was present at

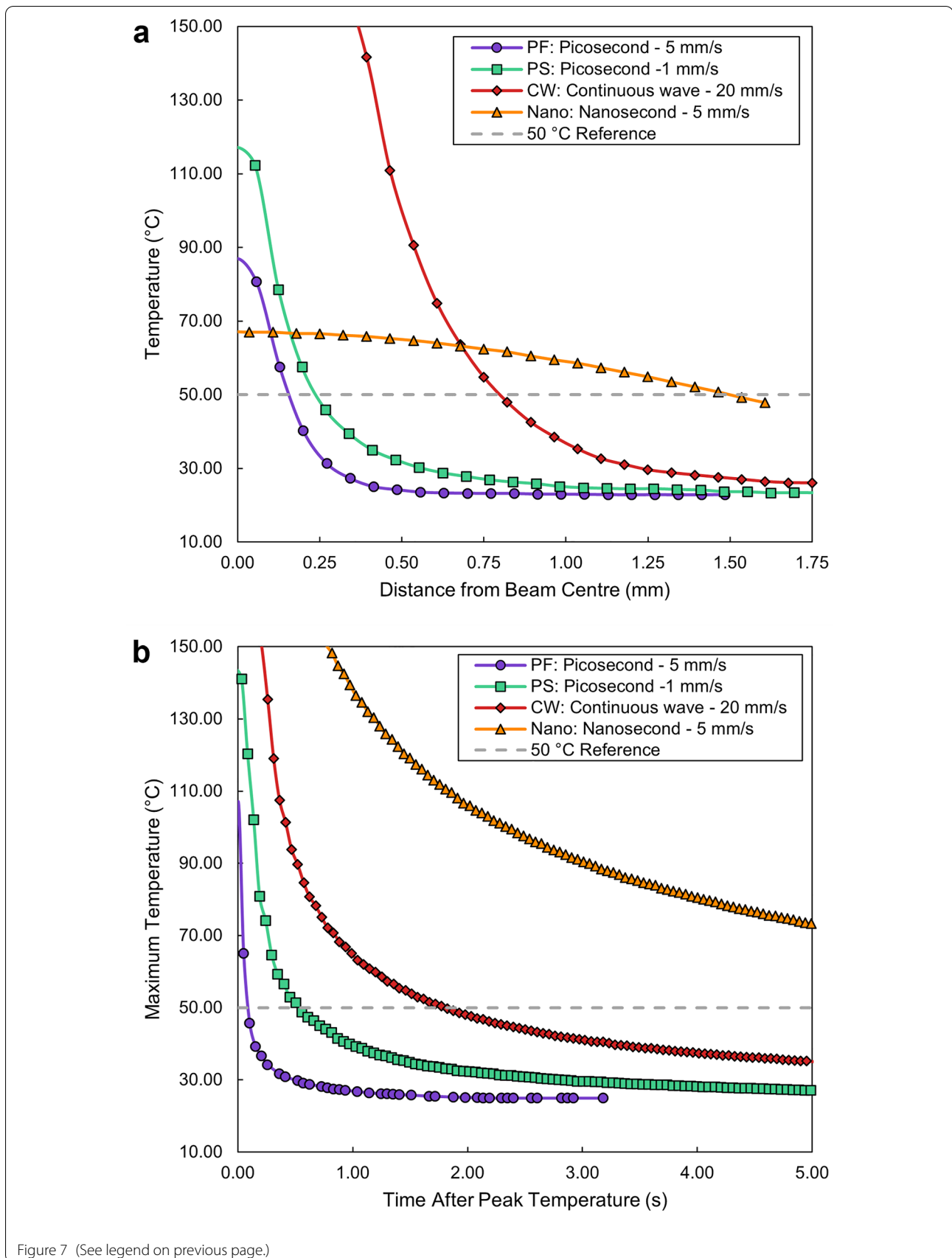
the beginning of the laser interaction (Figure 8(b)-(ii)), and during this period the bone was heated, initiating a melt pool (Figure 8(b)-(iii)). Further heating by the laser caused a bubble to form which also contained carbonised debris (Figure 8(b)-(iv)). The contents of the bubble were seen to be rotating and growing in volume over time. The bubble then overcame the surface tension of the surrounding melt pool and was ejected from the surface—removing both the molten material and carbonised debris. This difference in material removal mechanisms for a continuous wave laser and nanosecond pulsed laser highlights the transition from thermomechanical to thermal when longer/continuous pulse durations are used.

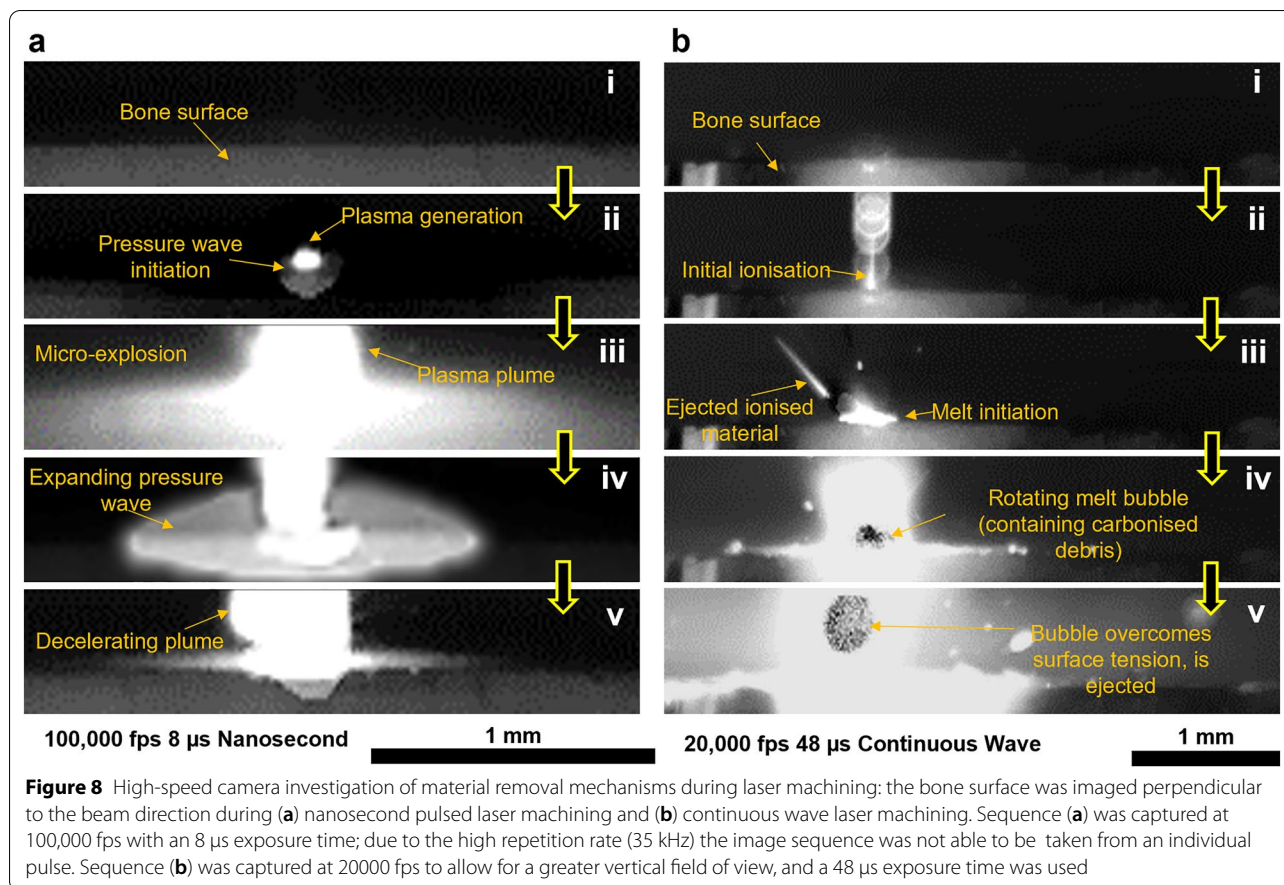
### 3.2 Necrotic Damage Assessment

Conventional machining processes (i.e., drilling, milling) have shown that temperatures as low as 50 °C can

(See figure on next page.)

**Figure 7** Investigation of thermal effects after laser machining: (a) the thermal penetration depth is plotted relative to the radial distance from the laser beam centre measured by infrared thermography. The profiles were selected from the recorded frame where the radial distance from the beam centre at a temperature greater than 50 °C was at a maximum. A 50 °C reference line is also plotted. (b) The cooling behaviour was studied through the use of temporal plots evaluating the maximum temperature along a radial profile from the beam centre relative to the time passed since peak temperature was achieved





produce necrotic damage in cortical bone if withheld for 30 seconds [17]; however, should larger temperatures occur, they will induce necrosis much faster. Nevertheless, in laser machining, the mechanical effect is removed due to the thermally dominant process that is laser ablation and as a result, heat generation can be enough to cause thermal necrosis in bone [25], but this can be minimised with the use of air and water spraying during the laser cutting process [29]. While the use of coolants is necessary in clinical environments as a precautionary measure for necrosis avoidance, in a research environment it does not allow a straight-forward analysis of the material response to different types of lasers. Thus, with the intention of studying the effect that the native laser (i.e., without any coolant) could have on the tissue in

terms of thermally induced necrosis, the samples were assessed with histological analysis (see Figure 9). Necrosis was evaluated by measuring the normal distance from the trench site until the extent within the tissue at which the lacunae stopped from being empty (i.e., with dead osteocytes) to being filled (i.e., with osteocytes).

It is observed that a larger temperature does not necessarily imply a larger necrotic depth if the acting time of the temperature is short (Table 3). Machining with the picosecond laser at 5 mm/s (PF) produced a maximum temperature of 122 °C and resulted in a necrotic depth of  $79 \pm 7 \mu\text{m}$ , while also depicting the shallowest trench (Figure 9(b)). Slowing down the feed rate by 5 times (i.e., 1 mm/s, PS) produced a maximum temperature of 143 °C and a necrotic depth of  $190 \pm 39 \mu\text{m}$  (Figure 9(c)), clearly

(See figure on next page.)

**Figure 9** Histological analysis for necrosis assessment: the necrotic depth was assessed by measuring the normal distance from the trench profile to the dashed black line, which marks the interface between the zone with empty lacunae (i.e., necrotic zone) and the zone with filled lacunae (i.e., necrosis-free zone): (a) Control sample free of necrosis, as all lacunae are filled with osteocytes, (b) Picosecond laser machining at 5 mm/s (PF) exhibits a necrotic depth of  $79 \pm 7 \mu\text{m}$ , while also depicting the smallest trench, (c) picosecond laser machining at 1 mm/s (PS) shows a necrotic depth  $190 \pm 39 \mu\text{m}$  and shows a trench depth that almost reached the bottom of the sample, (d) continuous wave laser machining at 20 mm/s caused a necrotic depth of  $194 \pm 19 \mu\text{m}$ , which is similar to the one in c, but in this case the trench is much shallower, (e) nanosecond laser machining at 5 mm/s showed a necrotic depth of  $268 \pm 67 \mu\text{m}$ , while also exhibiting a deep trench and carbonisation traits in the trench profile

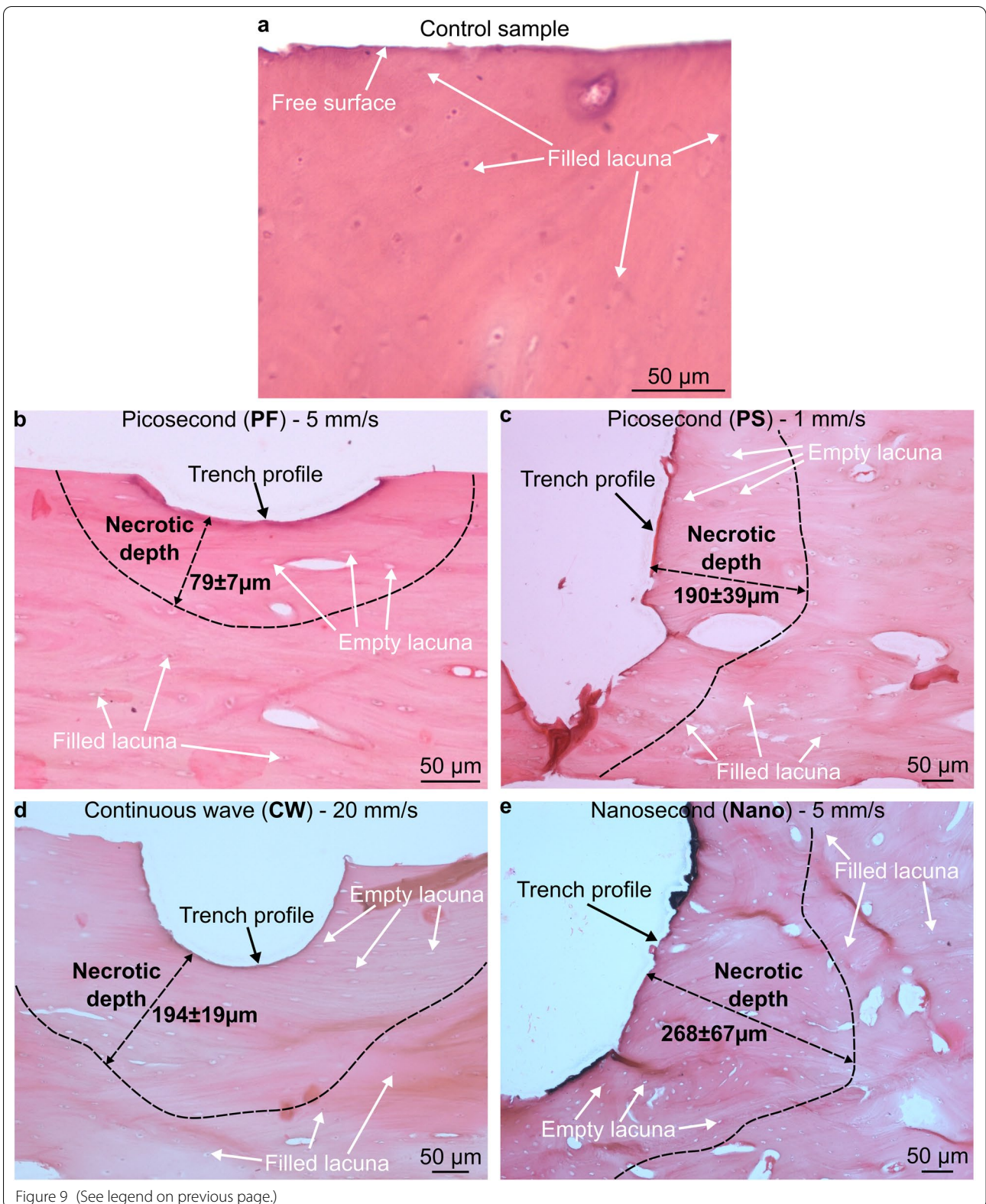


**Table 3** Necrotic depth for all the laser conditions

Alias	Laser	Feed, $F$ (mm/s)	$T_{max}$ (°C)	Duration of sample above 50 °C (s)	Necrotic depth ( $\mu\text{m}$ ), avg $\pm$ std. dev.	Number of measurements, $n$
PF	Picosecond	5	122	0.085	$79 \pm 7$	48
PS	Picosecond	1	143	0.530	$190 \pm 39$	56
CW	Continuous wave	20	1318	1.790	$194 \pm 19$	52
Nano	Nanosecond	5	830	11.000	$268 \pm 67$	62

showing that a longer exposure to same-power laser will inherently facilitate temperature build-up and, therefore, increase necrosis. The continuous wave laser at 20 mm/s feed (CW) produced the highest temperature of all tests with a maximum value of 1318 °C, but the necrotic depth was not the greatest, with a value very close to that achieved in PS conditions:  $194 \pm 19 \mu\text{m}$  (Figure 9(d)). Cutting at 5 mm/s with the nanosecond laser (Nano) produced a temperature of 813 °C, which resulted in the largest necrotic value of  $268 \pm 67 \mu\text{m}$  (Figure 9(d)). Note how even when the PS produced a larger maximum temperature than the Nano, the nanosecond laser produced carbonisation in the tissue, which is visible along the trench profile in Figure 9e; phenomenon that is not visible in (Figure 9(c)). Thus, this inherently shows that the necrosis is strongly affected by the laser power and acting time in tissue, but also proves that the pulse time of the laser will result in a different material response.

A separate control sample subjected to the same experimental conditions, but excepting the laser ablation process, was also assessed with histology to confirm that the handling, preparation, and storage processes did not induce necrosis to the tissue (Figure 9(a)). The evaluation showed no evidence of necrosis neither in the vicinity of the free surface nor in the bulk region of the sample, i.e., all the lacunae appear filled. Consequently, this confirms that the followed methodology is appropriate for this study and that the necrotic damage from PS, PE, CW and Nano samples was induced by the thermal effect of the laser machining process.

#### 4 Discussion

Bone machining under conventional methods such as milling, grinding, or sawing, involves the mechanical removal of material, which inherently produces a mixed thermomechanical process that induces damage to the tissue in various forms (e.g., cracks, mechanical properties decay, necrosis, carbonisation, etc.). Altogether, these forms of damage alter the bone regeneration capacity and the healing process (i.e., the remodelling process of the bone is hindered) [18], being also able to affect any implant bonding process [40].

An approach to reduce these types of damage is to use non-conventional machining techniques, such as laser machining. Here, the effect that the laser pulse width and the feed speed have on necrosis inducement and trench profile were explored. To do so, gold-standard technique of histology has been employed towards biological tissue analysis for necrosis assessment post-machining. Additionally, the trench profiles under various feed speeds and laser pulse widths were measured and analysed in accordance with the respective laser processing parameters.

The metrology assessment showed a non-linear relationship between the feed speed and trench depth (Figure 6) in all laser types (i.e., picosecond, nanosecond, and continuous wave). As found in the thermal analysis during machining (Figure 7(b)), the maximum temperature of the bone can be increased significantly in a rapid time period. With all the samples recording  $>100 \text{ }^\circ\text{C}$  temperatures, some vaporisation of the water, which is a key constituent of bone [41], would initially be expected from a purely thermal viewpoint. This would alter the composition of the bone so that there is a non-constant ratio of the volume of the constituent (e.g., water:collagen:hydroxyapatite), thus contributing to non-linear optical properties (i.e., the wavelength dependent optical absorption coefficient). The non-linear absorption characteristics have also been discussed in an investigation of laser machining trabecular bone [42], where it was theorised that the bone marrow, consisting of water and other organic material, would be vapourised in the initial stages because of their lower vaporisation temperature than that of hydroxyapatite.

Surface cracks propagating perpendicularly from the trench direction were also found in the slower picosecond sample ( $F = 1.0 \text{ mm/s}$ ) (Figure 4(b)). As the temperature in this sample was not raised to the elevated temperatures recorded after machining by the continuous wave and nanosecond laser, which did not show cracks, it is unlikely that thermally induced stresses were their cause. A more likely explanation is that the comparatively higher fluence (i.e., energy per unit area) of the picosecond laser ( $69.67 \text{ J/cm}^2$ ), when compared to the nanosecond laser ( $25.11 \text{ J/cm}^2$ ) with the longer pulse

width, was the source of these cracks. This high fluence and the high associated peak pulse power (picosecond = 14.6 MW, nanosecond = 2.6 kW) would introduce non-linear optical breakdown, where the increased photomechanical effect caused by the explosive generation of plasma—introducing cracks [43]. This theory is supported by the high-speed imaging investigation (Figure 8) where the nanosecond pulsed laser removed material by a thermomechanical mechanism as opposed to the continuous wave laser which was thermal. Combining these findings with those from the thermal investigations (Figure 7), it could be suggested that decreasing the pulse width further (i.e., to the picosecond region) would reduce the thermal effects seen in the nanosecond laser sample, transitioning to photomechanical effects instead. It is also interesting how the cracks were not present after picosecond laser machining with a faster feed speed ( $F = 4.0$  mm/s), potentially due to less dehydration of the bone coupled with the lower associated temperature increase preventing the bone becoming more brittle and therefore, less susceptible to crack initiation by the plasma induced pressure wave. This lack of thermal damage also suggests the promising possibility of using lasers with a short pulse width and higher feed speeds in a clinical setting to substantially minimise the necrotic depth observed in the lasers with a longer to continuous [44] pulse width.

Necrosis evaluation (Table 3) showed that the greatest necrotic depth occurred for the nanosecond (Nano) laser with a value of  $268 \pm 67$   $\mu\text{m}$ , which is an interesting outcome, given that the maximum temperature was recorded for a different laser (i.e., the CW laser reached a peak value of  $1318$   $^{\circ}\text{C}$  and necrotic depth of  $194 \pm 19$ ), while the Nano just reached a maximum of  $830$   $^{\circ}\text{C}$ . Nevertheless, by looking at Figure 7(a) the peak temperature drops to a necrotic threshold value (i.e.,  $50$   $^{\circ}\text{C}$ ) at ca.  $750$   $\mu\text{m}$  from the laser beam centre, while the Nano depicts a deeper propagation up to almost twice the distance ( $1500$   $\mu\text{m}$ ); thus, showing that even if the peak temperature was lower, it penetrated deeper into the bone. Additionally, from Figure 7(a), the Nano laser machining natural cooling time after laser exposure remained above  $50$   $^{\circ}\text{C}$  much longer than any of the other laser combinations used for histology (see Table 3). The reason for this is that the Nano laser frequency (35 kHz) in combination with the pulse energy of 0.52 J (see Table 1) results in the greatest laser energy input towards the bone (i.e., 12.81 J), even if the laser interaction time was not as great as with continuous wave. This implies that the nanosecond laser conditions employed, produced the greatest heat generation and heat transfer into the tissue, thus resulting in increased carbonisation and a higher necrotic depth.

It is interesting to note that the total input energy from the picosecond laser with slow feed (PS) also has a similar

input energy of 12.25 J; however, the necrotic depth for PS was evaluated as  $190 \pm 39$   $\mu\text{m}$ . The picosecond laser, having its pulse width about 3000 times shorter than the nanosecond, allows for a larger pulse energy and a lower frequency. Therefore, these conditions favour the natural convection that cools down the sample after each laser pulse; these is the reason why the PS and PF laser conditions produced the minimum necrosis values. It is also interesting that even when the feed speed was 5 times larger in PF against PS, the peak temperature was only lower by  $21$   $^{\circ}\text{C}$ ; however, the difference in necrotic depth is much more noticeable (i.e.,  $79 \pm 7$   $\mu\text{m}$  in PF vs.  $190 \pm 39$  in PS); in this case, being the faster feed the only difference, laser interaction time is minimised and therefore less temperature and necrosis will occur.

The increased heat generation after nanosecond laser machining may be explained by the frequency dependent pulse overlap. This can be demonstrated by comparing PF with Nano, with the respective frequencies of 4 kHz and 35 kHz, coupled with the spot sizes of  $40.0$   $\mu\text{m}$  and  $51.5$   $\mu\text{m}$ . In PF, there is an overlap of 96.9% ( $38.75$   $\mu\text{m}$ ) compared with 99.7% ( $51.36$   $\mu\text{m}$ ) in Nano. At the feed speeds in PF there are 32 individual pulses in the time taken to travel the distance of 1 spot diameter as opposed to 1802.5 in Nano, when also considering the pulse widths it becomes clearer how Nano suffers a longer cooling time.

When comparing the effect of PS and CW lasers in histology, the necrotic depth could be regarded as equal; even though there are evident differences in temperature behaviour (see Figure 9). The CW laser, while not allowing intermittent natural convection (i.e., cooling between each pulse), eases heat conduction through the tissue, which is why carbonisation occurred in CW and not in PS. The reason for achieving a similar necrotic depth could be that even if the total input energy from PS is 12.25 J (i.e., 4 times larger than that from CW), the laser interaction time is very little (i.e.,  $8.4 \times 10^{-7}$  s), while in CW the interaction time is 0.175 s. The drastic difference in laser interaction time between PS and CW (which is dependent on the pulse width and frequency) allows to achieve similar necrotic damage, but due to the large feed speed of CW (i.e., 20 times faster than PS), the machined trench is shallower than that from PS (see Figure 9(c), (d)).

In all cases, the peak temperature exceeded  $100$   $^{\circ}\text{C}$ , which could produce dehydration in the tissue [45] and therefore induce brittleness and micromechanical properties decay [7]. However, micromechanical properties evaluation is out of the scope of this research. Nevertheless, the exceedingly large temperatures here measured (i.e.,  $>800$   $^{\circ}\text{C}$  for Nano and CW lasers), even when only lasting a fraction of a second in the tissue, were high

enough to produce carbonisation in the tissue, another type of damage different from necrosis. Carbonisation traits, which are expected to be removed during the histological analysis processing, are even visible in the trench profile from the histological slices (see Figure 9(e)), which is coherent with this sample also exhibiting the greatest necrotic depth.

While it is known that laser machining of bone is a promising technique towards intelligent tooling systems for surgical interventions, laser processing parameters imperatively need optimisation to compete with conventional machining processes, which are characterised by a much larger material removal rate [33]. The findings from this research show that the pulse width in laser machining of bone plays a major role both in the surface quality, trench depth (i.e., which is related to the material removal rate) and in cellular damage (i.e., necrosis). Here, it is shown that greater energy density can be employed in the laser processing parameters only if narrower pulse widths are employed, but the frequency should be chosen to allow enough convection between each pulse. It is important to mention that this study is limited to dry machining (i.e., no external coolants were used to allow for a more native material response to various laser conditions) and was carried out in ex-vivo specimens.

## 5 Conclusions

An experimental study was performed to assess the surface quality (i.e., roughness, trench depth, cracks) and induced cellular damage (i.e., necrosis) in ex-vivo bovine cortical bone, following laser machining processes at various feed speeds (i.e., 1–20 mm/s) and laser pulse widths (i.e., 60 ps, 200 ns, continuous wave). Thermal measurements showed that peak temperatures during processing can reach up to 1318 °C for an instant, but the thermal distribution is affected by the cooling time (i.e., time between each pulse). Surface inspection showed that there is a non-linear relationship between feed speed and trench depth and a notably, a large depth variation over a small feed speed range for the nanosecond laser when compared to a similar feed range by the picosecond laser. Surface cracks were also found on the sample machined by the picosecond laser at a slow feed speed ( $F = 1.0$  mm/s), the absence of these cracks in the other samples indicates that their formation may be caused by the production of an explosive plasma pressure wave and is potentially exacerbated by dehydration of the bone. Histological analysis revealed that the 200 ns pulse width produced the greatest necrotic damage and carbonisation, whereas the 60 ps pulse width produced the

minimum; being the main reason that a shorter pulse width facilitates intermittent convection between each pulse (favoured cooling).

This study reveals how choice of laser type (i.e., pulsed or continuous wave) needs to be considered for the further development of laser osteotomy. Additionally, it exposes how pulse duration and frequency leads to large variations in the thermally induced effects imparted to the bone during machining. This highlights the potential for the use of ultra-short pulse widths (i.e., in the picosecond range) to shift the material removal mechanisms from thermal to optomechanical, reducing the temperature-dependent necrotic depth and in-turn, the opportunity to improve healing times in a clinical scope.

### Acknowledgements

This study was supported by Nottingham research fellowship programme and Beacons of Excellence. All the experimental (i.e., sample preparation, laser machining) and evaluation (i.e., metrology, histology) processes were conducted both in the Faculty of Engineering and the School of Life Sciences from University of Nottingham, UK. The authors would also like to thank the support from EPSRC through the DTP 2018–19 University of Nottingham (No: EP/T517902/1).

### Author Contributions

Jose A. Robles-Linares and Kieran Winter were in charge of the whole trial, writing the manuscript and data collection/analysis. Zhirong Liao conceived the research idea and reviewed/edited the manuscript. All authors read and approved the final manuscript.

### Authors' Information

Jose A. Robles-Linares, born in 1994, is currently a PhD candidate at the Advanced Manufacturing Technology research group, in the Mechanical, Materials and Manufacturing Department from the *Faculty of Engineering, University of Nottingham, UK*. He received his bachelor's degree in Mechanical Engineering from *CETYS Universidad, Mexicali, Mexico* and his MSc degree in Manufacturing Systems from *Tecnologico de Monterrey, Monterrey, Mexico*. His research interests include biomaterials, micromechanics and surface integrity. Kieran Winter, born in 1998 is currently a PhD candidate at the Advanced Manufacturing Technology research group, in the Mechanical, Materials and Manufacturing Department from the *Faculty of Engineering, University of Nottingham, UK*. He received his MEng in Manufacturing Engineering from University of Nottingham. His research interests include the non-conventional machining of magnetic materials and surface integrity. Zhirong Liao, born in 1987, is currently an associate professor in the Mechanical, Materials and Manufacturing Department from the Faculty of Engineering, University of Nottingham, UK. He received his BEng, MSc and PhD degree in Mechanical Engineering from Harbin Institute of Technology, China, in 2010, 2012 and 2017. His research interests include conventional and non-conventional machining, surface integrity and precision manufacturing.

### Funding

Supported by The University of Nottingham, the Mexican National Council for Science and Technology (CONACYT), EPSRC through the DTP 2018–19 University of Nottingham (Grant No. EP/T517902/1), Nottingham Research Fellowship and University of Nottingham Propulsion Futures Beacon Programme.

### Competing Interests

The authors declare no competing financial interests.

Received: 23 June 2021 Revised: 2 March 2022 Accepted: 26 April 2022  
Published online: 20 May 2022

## References

- [1] S L Croker, J G Clement, D Donlon. A comparison of cortical bone thickness in the femoral midshaft of humans and two non-human mammals, *HOMO. J. Comp. Hum. Biol.*, 2009, 60: 551–565. <https://doi.org/10.1016/j.jchb.2009.07.003>.
- [2] Z Liao, D A Axinte. On monitoring chip formation, penetration depth and cutting malfunctions in bone micro-drilling via acoustic emission. *J. Mater. Process. Technol.*, 2016, 229: 82–93. <https://doi.org/10.1016/j.jmatp.rotec.2015.09.016>.
- [3] Z Liao, D A Axinte. On chip formation mechanism in orthogonal cutting of bone. *Int. J. Mach. Tools Manuf.*, 2016, 102: 41–55. <https://doi.org/10.1016/j.jmachtools.2015.12.004>.
- [4] Z Liao, D Axinte, D Gao. On modelling of cutting force and temperature in bone milling. *J. Mater. Process. Technol.*, 2019, 266: 627–638. <https://doi.org/10.1016/j.jmatp.rotec.2018.11.039>.
- [5] Y Zhang, J A Robles-Linares, L Chen, et al. Advances in machining of hard tissues – From material removal mechanisms to tooling solutions. *Int. J. Mach. Tools Manuf.*, 2022, 172: 103838. <https://doi.org/10.1016/j.jmachtools.2021.103838>.
- [6] J F Yin, Q Bai, B Zhang, Methods for detection of subsurface damage: A review. *Chinese J. Mech. Eng.*, 2018, 31: 41. <https://doi.org/10.1186/s10033-018-0229-2>.
- [7] J A Robles-Linares, D Axinte, Z Liao, et al. Machining-induced thermal damage in cortical bone: Necrosis and micro-mechanical integrity. *Mater. Des.*, 2021, 197: 109215. <https://doi.org/10.1016/j.matdes.2020.109215>.
- [8] S Zhang, J Zhang, B Zhu, et al. Progress in Bio-inspired anti-solid particle erosion materials: Learning from nature but going beyond nature. *Chinese J. Mech. Eng.*, 2020, 33: 42. <https://doi.org/10.1186/s10033-020-00458-y>.
- [9] Z Liao, D A Axinte, D Gao. A novel cutting tool design to avoid surface damage in bone machining. *Int. J. Mach. Tools Manuf.*, 2017, 116: 52–59. <https://doi.org/10.1016/j.jmachtools.2017.01.003>.
- [10] L Shu, S Li, M Terashima, W Bai, et al. A novel self-centring drill bit design for low-trauma bone drilling. *Int. J. Mach. Tools Manuf.*, 2020, 154: 103568. <https://doi.org/10.1016/j.jmachtools.2020.103568>.
- [11] J Robles-Linares, E Ramirez-Cedillo, H Siller, et al. Parametric modeling of biomimetic cortical bone microstructure for additive manufacturing. *Materials* (Basel), 2019, 12: 913. <https://doi.org/10.3390/ma12060913>.
- [12] S C Cowin, L Cardoso. Blood and interstitial flow in the hierarchical pore space architecture of bone tissue. *J. Biomech.*, 2015, 48: 842–854. <https://doi.org/10.1016/j.jbiomech.2014.12.013>.
- [13] J A R Linares-Alvelais, J Obedt Figueroa-Cavazos, C Chuck-Hernandez, et al. Hydrostatic high-pressure post-processing of specimens fabricated by DLP, SLA, and FDM: An alternative for the sterilization of polymer-based biomedical devices. *Materials* (Basel). 2018, 11: <https://doi.org/10.3390/ma11122540>.
- [14] C Tan, J Zou, S Li, et al. Additive manufacturing of bio-inspired multi-scale hierarchically strengthened lattice structures. *Int. J. Mach. Tools Manuf.*, 2021, 167: 103764. <https://doi.org/10.1016/j.jmachtools.2021.103764>.
- [15] N M Hancox. *Biology of Bone*. 1st ed. Cambridge University Press, Cambridge, 1972.
- [16] W Bai, L Shu, R Sun, et al. Mechanism of material removal in orthogonal cutting of cortical bone. *J. Mech. Behav. Biomed. Mater.*, 2020: 103618. <https://doi.org/10.1016/j.jmbbm.2020.103618>.
- [17] G Augustin, S Davila, K Mihoci, et al. Thermal osteonecrosis and bone drilling parameters revisited. *Arch. Orthop. Trauma Surg.*, 2008, 128: 71–77. <https://doi.org/10.1007/s00402-007-0427-3>.
- [18] M Mediouni, T Kucklick, S Poncet, et al. An overview of thermal necrosis: present and future. *Curr. Med. Res. Opin.*, 2019, 35: 1555–1562. <https://doi.org/10.1080/03007995.2019.1603671>.
- [19] D Cha, D Axinte, J Billingham. Geometrical modelling of pulsed laser ablation of high performance metallic alloys. *Int. J. Mach. Tools Manuf.*, 2019, 141: 78–88. <https://doi.org/10.1016/j.jmachtools.2019.04.004>.
- [20] V Villerius, H Kooiker, J Post, et al. Ultrashort pulsed laser ablation of stainless steels. *Int. J. Mach. Tools Manuf.*, 2019, 138: 27–35. <https://doi.org/10.1016/j.jmachtools.2018.11.003>.
- [21] K W Baek, W Deibel, D Marinov, et al. Clinical applicability of robot-guided contact-free laser osteotomy in craniomaxillo-facial surgery: In-vitro simulation and in-vivo surgery in minipig mandibles. *Br. J. Oral Maxillofac. Surg.*, 2015, 53: 976–981. <https://doi.org/10.1016/j.bjoms.2015.07.019>.
- [22] S Amini-Nik, D Kraemer, M L Cowan, et al. Ultrafast mid-IR laser scalpel: Protein signals of the fundamental limits to minimally invasive surgery. *PLoS One.*, 2010, 5: e13053. <https://doi.org/10.1371/journal.pone.0013053>.
- [23] A Feldmann, P Wili, G Maquer, et al. The thermal conductivity of cortical and cancellous bone. *Eur. Cells Mater.*, 2018, 35: 25–33. <https://doi.org/10.22203/eCM.v035a03>.
- [24] A Vogel, V Venugopalan. Mechanisms of Pulsed laser ablation of soft biological tissues. *Chem. Rev.*, 2003, 103: 577–644. [https://doi.org/10.1007/978-90-481-8831-4\\_14](https://doi.org/10.1007/978-90-481-8831-4_14).
- [25] L S Krause, C M Cobb, J W Rapley, et al. Laser irradiation of bone. I. an in vitro study concerning the effects of the CO<sub>2</sub> laser on oral mucosa and subjacent bone. *J. Periodontol.*, 1997, 68: 872–880. <https://doi.org/10.1902/jop.1997.68.9.872>.
- [26] Y Liu, D Luo, T Wang. Hierarchical structures of bone and bioinspired bone tissue engineering. *Small*, 2016, 12: 4611–4632. <https://doi.org/10.1002/smll.201600626>.
- [27] H Nguendon Kenhagho, F Canbaz, T E Gomez Alvarez-Arenas, et al. Machine learning-based optoacoustic tissue classification method for laser osteotomies using an air-coupled transducer. *Lasers Surg. Med.*, 2021, 53: 377–389. <https://doi.org/10.1002/lsm.23290>.
- [28] G M Rayan, D T Stanfield, S Cahill, et al. Effects of rapid pulsed CO<sub>2</sub> laser beam on cortical bone in vivo. *Lasers Surg. Med.*, 1992, 12: 615–620. <https://doi.org/10.1002/lsm.1900120608>.
- [29] M Frenzen, W Götz, M Ivanenko, et al. Osteotomy with 80- $\mu$ s CO<sub>2</sub> laser pulses - Histological results. *Lasers Med. Sci.*, 2003, 18: 119–124. <https://doi.org/10.1007/s10103-003-0264-8>.
- [30] D G Pandurić, I Bago, D Katanec, et al. Comparison of Er:YAG Laser and surgical drill for osteotomy in oral surgery: An experimental study. *J. Oral Maxillofac. Surg.*, 2012, 70: 2515–2521. <https://doi.org/10.1016/j.joms.2012.06.192>.
- [31] K W Baek, W Deibel, D Marinov, et al. A comparative investigation of bone surface after cutting with mechanical tools and Er:YAG laser. *Lasers Surg. Med.*, 2015, 47: 426–432. <https://doi.org/10.1002/lsm.22352>.
- [32] L Beltran, H Abbasi, R Georg, et al. Effect of laser pulse duration on ablation efficiency of hard bone in microsecond regime. M.F.P. Martins Costa (Ed.), *Third Int. Conf. Appl. Opt. Photonics*, SPIE, 2017: 115. <https://doi.org/10.1117/12.2272253>.
- [33] L M Beltran Bernal, I T Schmidt, N Vulin, et al. Optimizing controlled laser cutting of hard tissue (bone). *Autom.*, 2018, 66: 1072–1082. <https://doi.org/10.1515/auto-2018-0072>.
- [34] M A K Liebschner. Biomechanical considerations of animal models used in tissue engineering of bone. *Biomaterials*, 2004, 25: 1697–1714. [https://doi.org/10.1016/S0142-9612\(03\)00515-5](https://doi.org/10.1016/S0142-9612(03)00515-5).
- [35] J C H Goh, E J Ang, K Bose. Effect of preservation medium on the mechanical properties of cat bones. *Acta Orthop.*, 1989, 60: 465–467. <https://doi.org/10.3109/17453678909149321>.
- [36] G Zhang, X Deng, F Guan, et al. The effect of storage time in saline solution on the material properties of cortical bone tissue. *Clin. Biomech.*, 2018, 57: 56–66. <https://doi.org/10.1016/j.clinbiomech.2018.06.003>.
- [37] A Feldmann, P Zysset. Experimental determination of the emissivity of bone. *Med. Eng. Phys.*, 2016, 38: 1136–1138. <https://doi.org/10.1016/j.medengphy.2016.06.019>.
- [38] Z Liao, A la Monaca, J Murray, et al. Surface integrity in metal machining - Part I: Fundamentals of surface characteristics and formation mechanisms. *Int. J. Mach. Tools Manuf.*, 2021, 162: 103687. <https://doi.org/10.1016/j.jmachtools.2020.103687>.
- [39] A la Monaca, J W Murray, Z Liao, et al. Surface integrity in metal machining - Part II: Functional performance. *Int. J. Mach. Tools Manuf.*, 2021, 164: 103718. <https://doi.org/10.1016/j.jmachtools.2021.103718>.
- [40] D Axinte, Y Guo, Z Liao, et al. Machining of biocompatible materials — Recent advances. *CIRP Ann.*, 2019, 68: 629–652. <https://doi.org/10.1016/j.cirp.2019.05.003>.
- [41] G D Rajitha Gunaratne, R Khan, D Fick, et al. A review of the physiological and histological effects of laser osteotomy. *J. Med. Eng. Technol.*, 2017, 41: 1–12. <https://doi.org/10.1080/03091902.2016.1199743>.
- [42] M V Pantawane, R T Chipper, W B Robertson, et al. Evolution of surface morphology of Er:YAG laser-machined human bone. *Lasers Med. Sci.*, 2020, 35: 1477–1485. <https://doi.org/10.1007/s10103-019-02927-w>.

- [43] Y Sotsuka, S Nishimoto, T Tsumano, et al. The dawn of computer-assisted robotic osteotomy with ytterbium-doped fiber laser. *Lasers Med. Sci.*, 2014, 29: 1125–1129. <https://doi.org/10.1007/s10103-013-1487-y>.
- [44] J T Payne, G M Peavy, L Reinisch, et al. Cortical bone healing following laser osteotomy using 6.1  $\mu\text{m}$  wavelength. *Lasers Surg. Med.*, 2021, 29: 38–43. <https://doi.org/10.1002/lsm.1084>.
- [45] J Samuel, J S Park, J Almer, et al. Effect of water on nanomechanics of bone is different between tension and compression. *J. Mech. Behav. Biomed. Mater.*, 2016, 57: 128–138. <https://doi.org/10.1016/j.jmbbm.2015.12.001>.

**Submit your manuscript to a SpringerOpen<sup>®</sup> journal and benefit from:**

- ▶ Convenient online submission
- ▶ Rigorous peer review
- ▶ Open access: articles freely available online
- ▶ High visibility within the field
- ▶ Retaining the copyright to your article

---

Submit your next manuscript at ▶ [springeropen.com](https://www.springeropen.com)

---